

Optical absorption induced by small polaron formation in transition metal oxides: The case of Co_3O_4 Tyler J. Smart,^{1,2} Tuan Anh Pham,² Yuan Ping ^{3,*} and Tadashi Ogitsu^{2,†}¹Department of Physics, University of California Santa Cruz, Santa Cruz, California 95064, USA²Quantum Simulations Group, Lawrence Livermore National Laboratory, Livermore, California 94551, USA³Department of Chemistry and Biochemistry, University of California Santa Cruz, Santa Cruz, California 95064, USA

(Received 17 July 2019; revised manuscript received 14 September 2019; published 14 October 2019)

Small polarons (SPs) are known to exist in most important transition metal oxides; however, the nature of small polaron formation remains enigmatic, and a fundamental understanding of how SPs impact the intrinsic electronic structure and optical properties of these materials is largely lacking. In this work, we employ first-principles calculations to investigate SP formation in Co_3O_4 , a highly promising material for a wide range of emerging energy applications, and we resolve the conflicting findings that have been reported on the electronic structure of the system. We confirm that the intrinsic band gap of Co_3O_4 is 1.6 eV, and we show that the formation of small hole polarons significantly influences the optical absorption spectra, leading to a 0.8 eV transition that is often misinterpreted as the band edge that defines the fundamental gap. In addition, we discuss how uniaxial strain can be utilized to probe the Jahn-Teller distortion of SP states and, in turn, effect their optical transitions. Beyond Co_3O_4 , our study suggests a general roadmap for establishing a first-principles computational approach that can simultaneously achieve an accurate description of SP states, electronic band structure, and optical transitions of polaronic magnetic oxides.

DOI: [10.1103/PhysRevMaterials.3.102401](https://doi.org/10.1103/PhysRevMaterials.3.102401)

Polarons, conduction electrons, or holes with self-induced lattice polarization are known to exist in most transition metal oxides (TMO) and deeply affect their optical and carrier transport properties [1]. In these materials, much of the interest has been related to the role of small polarons (SPs) that form when the induced lattice polarization is localized in a volume on the order of the unit cell. In particular, for many important TMOs, including Fe_2O_3 [2–4], NiO [5,6], Co_3O_4 [7,8], MnO [9], BiVO_4 [10–13], and CuO [14,15], it has been found that the formation of SPs is responsible for the low carrier mobility and conductivity, which hinders their practical application as electrochemical catalysts and photoelectrochemical (PEC) electrodes [16–20]. It is also well established that the transport of SPs in these TMOs can be characterized through the thermally activated hopping conduction mechanism and a logarithmic temperature dependence of the materials carrier mobility [21].

Unlike the distinct signature of SPs on the carrier conduction discussed above, the effect of polarons on electronic structure and optical transitions in TMOs is rather complex and difficult to elucidate. For example, in several TMOs, such as WO_3 [22,23], TiO_2 [24–26], and SrTiO_3 [27,28], the presence of large polarons that are delocalized over several unit cells may lead to a strong band gap renormalization through electron-phonon coupling. By contrast, the formation of SPs may introduce isolated gap states away from the band edges due to their spatially localized nature, which could be easily misinterpreted as band edges that define the fundamental band gap. A prime example is Fe_2O_3 , where recent time-resolved

spectroscopy experiments have shown that its midgap states are indeed associated with optically active polarons, which in turn lead to transition energies that are significantly lower than the fundamental band gap [29,30]. This conclusion is also consistent with Lohaus *et al.* [31], where the authors showed that while the band gap of Fe_2O_3 is 2.2 eV, an effective gap of 1.75 eV is observed due to the formation of small polarons. Nonetheless, distinguishing midgap states due to SP formation from other sources such as defect-bound states [32–34] and surface states [35] is still not well understood in the literature. Despite extensive experiments on these TMOs, theoretical studies of SP effects on electronic structure and optical properties of TMOs are limited. More importantly, challenges remain in first-principles methods that accurately describe polarons and the electronic structure of TMOs.

In this paper, we discuss the role of SPs (hereinafter referred to as “polarons” for simplicity) in trivalent tetraoxide (Co_3O_4), an antiferromagnetic oxide with a normal spinel structure. Despite that Co_3O_4 has been extensively investigated for a wide range of technologies [7,8,36–41], a fundamental understanding of the optical properties of this material remains largely lacking, and conflicting results have been reported, e.g., for the band gap of bulk Co_3O_4 . For instance, a value of 1.5–1.7 eV has been commonly reported for the optical gap of Co_3O_4 [42–48]. On the other hand, several experimental studies conclude that, despite a transition being observed around 1.5–1.7 eV, the true band gap of Co_3O_4 is significantly smaller, yielding a value of around 0.7–0.9 eV [49–52]. This conclusion, however, is not supported by time-resolved optical spectroscopy measurements, which suggest the state at ~ 0.8 eV above the valence band maximum is a localized polaron state [43,44,53]. Along this direction, other experiments have indicated that the intrinsic carriers in

*yuanping@ucsc.edu

†ogitsu1@llnl.gov

Co_3O_4 are hole polarons that are characterized by a nearest-neighbor hopping conduction mechanism and such a signature implies that hole polarons may affect the optical properties of Co_3O_4 in a similar way as in Fe_2O_3 [42,45,48,54–58]. Collectively, the existing results indicate that much is left to be understood regarding the nature of the optical transitions near the band edge of Co_3O_4 , and how it is related to polaron formation.

The aim of this work is to resolve the conflicting results in the literature on Co_3O_4 , and provide a coherent description of its electronic structure, carrier conduction, and optical properties through first-principles calculations. In particular, we discuss the level of theory needed for a proper description of the electronic structure of the material. In addition, we elucidate the role of polaron formation on the electronic band gap and optical spectra of p -doped Co_3O_4 , and we discuss how uniaxial strain can be used to distinguish polaron related transitions in the optical spectra. This work provides a straightforward method for considering SP effects in the first-principles calculations of optical absorption, alongside unambiguous SP peak assignment in agreement with previous experimental studies of Co_3O_4 . Furthermore, our study distinguishes the role of SP formation from other optical factors that are often considered in the literature (e.g., exciton formation, thermal broadening of optical spectra, and electron-phonon renormalization of band edges). Beyond Co_3O_4 our study presents a roadmap for first-principles calculations in the investigation of SP effects on the optical properties of TMOs.

We begin by discussing our computational strategy for addressing the electronic properties of Co_3O_4 (spinel structure shown in Fig. 1). It is well known that density functional theory (DFT), with conventional local or semilocal exchange-correlation functionals, is not sufficient to provide a proper description of polarons in transition metal oxides and often severely underestimates the band gap of these materials [59]. In order to mitigate this issue, several approaches have been

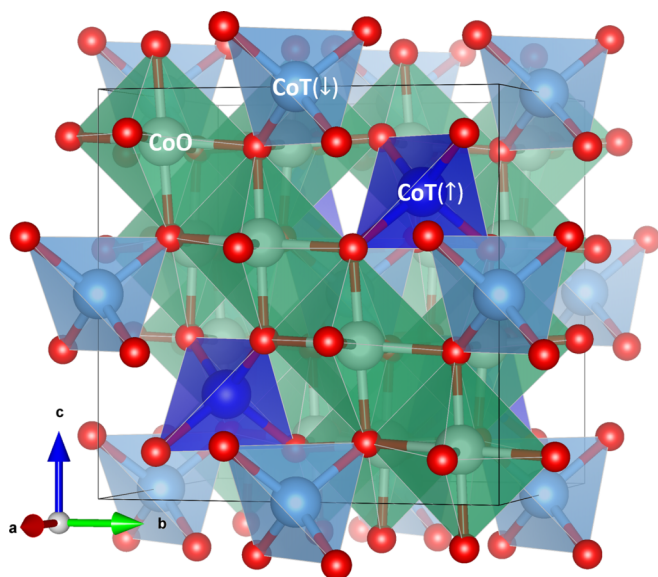


FIG. 1. Normal spinel atomic structure of Co_3O_4 . Octahedral Co are shown in green, tetrahedral Co are shown in blue/light blue (distinguishing spin polarization direction), and O are shown in red.

proposed, including DFT+ U with an orbital specific Hubbard U correction, and hybrid functional that includes a fraction of Hartree-Fock exchange (α), hereinafter denoted as PBE0(α). However, these calculations are known to highly depend on the choice of the Hartree-Fock exchange or Hubbard U correction. For instance, a wide range between 0.8 and 2.0 eV has been reported in the literature for the band gap of Co_3O_4 , depending on the level of theory employed [50]. In this context, it is also necessary to emphasize that, despite the significant development that has been made, establishing a first-principles approach that allows for an accurate prediction of the electronic properties of TMOs remains a significant challenge [60].

Here, we implement both hybrid functional and DFT+ U calculations to provide an unbiased description of the electronic properties of Co_3O_4 . Notably, in variation with previous hybrid functional calculations, we invoked the generalized Koopmans' condition to determine the value of α from first principles. We stress that this strategy has been shown to accurately predict the band gap of materials with band gaps up to 14 eV and has been particularly successful for polaronic systems [61–64]. Specifically, the generalized Koopmans' condition enforces the condition $\text{IP}_q = \text{EA}_{q+1}$ at a fixed geometry for an isolated state in the materials, where IP_q is the ionization potential of an occupied state at the charge state q , whereas EA_{q+1} is the electron affinity of the same state when it is unoccupied at the charge state $q + 1$. Here, we determine the value of α by enforcing the condition $\text{IP}_q = \text{EA}_{q+1}$ for both the hole and electron polaron [see Fig. S1 for more details of the electron polaron located in the Supplemental Material (SM) [65]], and we obtained a value of 0.12 for the Hartree-Fock exchange α in both cases, as shown in Fig. 2.

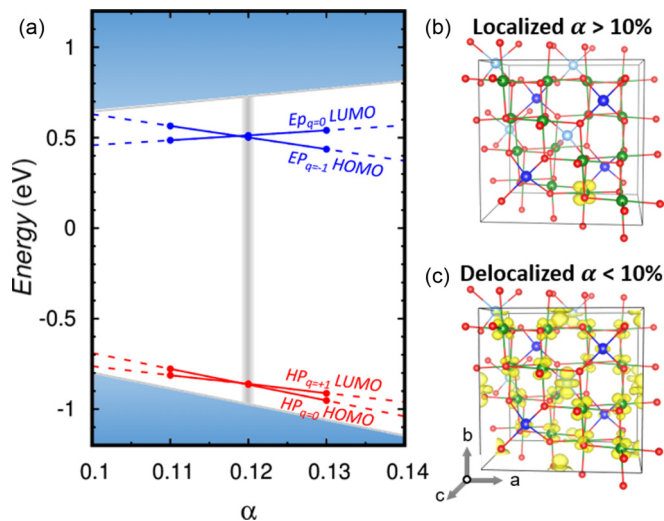


FIG. 2. (a) Generalized Koopmans' condition for electron polaron (EP) and hole polaron (HP) in Co_3O_4 . The exact exchange α for the PBE0(α) method is varied until the condition $\text{HOMO}_q = \text{LUMO}_{q+1}$ (at fixed geometry where polaron has formed) is met. In both cases, we find that at an exact exchange of 0.12 Koopmans' condition is satisfied. The corresponding pristine gap is computed to be 1.70 eV. (b) Localized and (c) delocalized hole wave function, subject to the value of the exact exchange. Isosurface plots use a cutoff of 10% the maximum.

We note that hole polarons do not form for α below 10%, as illustrated in Figs. 2(b) and 2(c). The value of α determined in this manner is an intrinsic property of the bulk system, and the choice of defect used to enforce the Koopmans' condition is proper as long as it has minimum hybridization with the bulk Bloch states [61,62,66].

We then determined U parameters based on the hybrid functional results, and the stable formation of electron and hole polarons (see Table S1 for more details). In particular, we find that the use of U values of $U_{\text{Co(O)}} = 4$ eV and $U_{\text{Co(T)}} = 3$ eV provides consistent results with Koopmans' compliant hybrid functional (band gap agrees within 0.1 eV), as well as a proper description of the electronic properties of the system, as discussed later in this Rapid Communication. We also note that hole polarons do not form for U values below 2.5 eV (see Fig. S2).

All the calculations were then carried out using the plane-wave code QUANTUM ESPRESSO [67] with norm-conserving pseudopotentials [68]. A plane wave cutoff of 100 Ry was used in all PBE+ U calculations, while a reduced cutoff of 50 Ry was implemented for the more demanding hybrid functional calculations (geometry and electronic structure are converged at 50 Ry). The calculations were generally performed within the 56 atom cubic cell with a $2 \times 2 \times 2$ k -point mesh for integration over the Brillouin zone. In addition, a $\sqrt{2} \times \sqrt{2} \times 2$ supercell with 224 atoms was utilized for comparison, particularly to understand the finite-size effects on polaron formation. Nevertheless, we find that the wave function character, energy level splitting, and band structure look largely unchanged between the 56 atom cubic cell and the 224 atom supercell (see Fig. S3 for further details). In all calculations with electron or hole polarons, the charged cell correction scheme as developed in Ref. [69] was employed, which is necessary in order to remove the spurious interactions of the polarons with their periodic images and with the uniform compensating background charge [70]. For the rest of the manuscript, unless otherwise noted, the results presented here were obtained at the DFT+ U level of theory that is computationally less demanding compared to hybrid functional calculations.

To set a baseline for the discussion of polaron effects in Co_3O_4 , we briefly summarize the electronic structure of the pristine system. As shown in Fig. 1, Co_3O_4 assembles in a normal spinel structure, where two-thirds of Co occupy octahedral sites [denoted by Co(O)] and the remaining third occupy tetrahedral sites [denoted by Co(T)]. We find that Co(O) exhibits a low-spin $3d^6$ orbital configuration with the O_h symmetry, leading to filled t_{2g} and empty e_g bands, as shown in the calculated projected density of states (PDOS) and band diagram presented in Figs. 3(a) and 3(b). On the other hand, Co(T) with the T_d symmetry forms a high-spin $3d^7$ configuration with a half-filled e_g band, yielding an overall magnetic moment of $\sim 3.2\mu_B$ as already reported in experiments [71]. These Co(T) sites experience an antiferromagnetic interaction mediated through a superexchange of mutually bonded oxygen; in addition, the presence of a large Hund's spin exchange results in a splitting of the t_2 band. This is shown in Figs. 3(c) and 3(d), where we find that the t_2 minority spin states are formed at a higher energy level, whereas all majority spin states occur at lower and similar

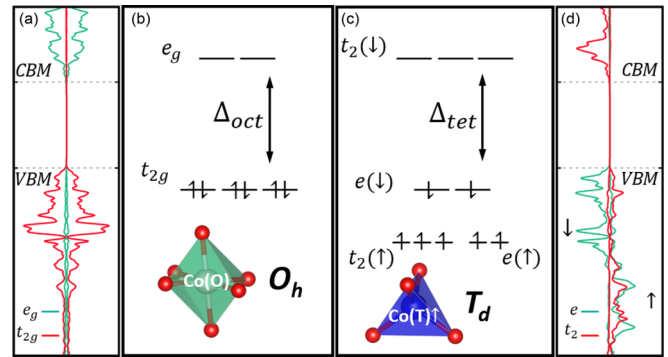


FIG. 3. (a) Projected density of states (PDOS) of Co(O) on t_{2g} and e_g orbitals. Schematic representation of the electronic configuration of (b) octahedral Co^{3+} and (c) tetrahedral Co^{2+} in Co_3O_4 due to a crystal field splitting (Δ_{oct} and Δ_{tet} , respectively). (d) PDOS of Co(T) on t_2 and e orbitals. All the PDOS were computed with DFT+ U .

energies [47,72] (also see Fig. S4 for further details). Overall, the behavior of the spin states and band splitting presented here are consistent with results reported in existing theoretical studies [72,73].

Next, we discuss the nature of polaron formation in Co_3O_4 . Our calculations show that, among the Co(O) and Co(T) sites where hole polarons can form, the total energy of a hole polaron forming at Co(O) is lower than that of Co(T) by at least 70 meV. A more stable formation of the polaron on Co(O) is also reflected in the calculated density of states of Co_3O_4 , where a larger contribution of Co(O) d states is found at the valence band edge compared to the Co(T) d states (see Fig. S4). Finally, our conclusion is consistent with the experimental study reported by Ngamou *et al.* [54], where the authors show that the hopping of polarons takes place in the octahedral sites and is responsible for driving the electrical transport in the oxide. Collectively, these results indicate that the computational approach employed here provides a proper description of polaron formation in Co_3O_4 .

Beyond the findings on the thermodynamical stability of hole polaron formation in Co_3O_4 , our calculations show that the hole polaron at Co(O) leads to several midgap states. As shown in Fig. 4, we find that, upon the hole polaron formation, Jahn-Teller (JT) distortion occurs at the Co(O) site due to an uneven occupation of the t_{2g} band and splits the degeneracy of the O_h states. In addition, the uneven occupation of up/down states splits the spin degeneracy due to the on-site Coulomb repulsion of the d orbitals. Specifically, we find that the majority spin states [e.g., $b_2(\uparrow)$, $a_1(\uparrow)$, $b_1(\uparrow)$] are located at a lower energy, whereas the minority spin states [e.g., $b_2(\downarrow)$, $a_1(\downarrow)$, $b_1(\downarrow)$] are pushed higher in the energy. Such splitting and ordering is consistent with the previous time-resolved spectroscopy measurements of Co(O) [46,73]. In addition, these midgap states are consistent with the experiment reported in Ref. [43], where it was found that midgap excitations are associated with $a_1(\uparrow)$ and $b_1(\uparrow)$ states of Co(O). As a result, our analyses point to significant effects of hole polarons on the electronic structure of Co_3O_4 , most notably in the formation of midgap states in a similar way as found in Fe_2O_3 .

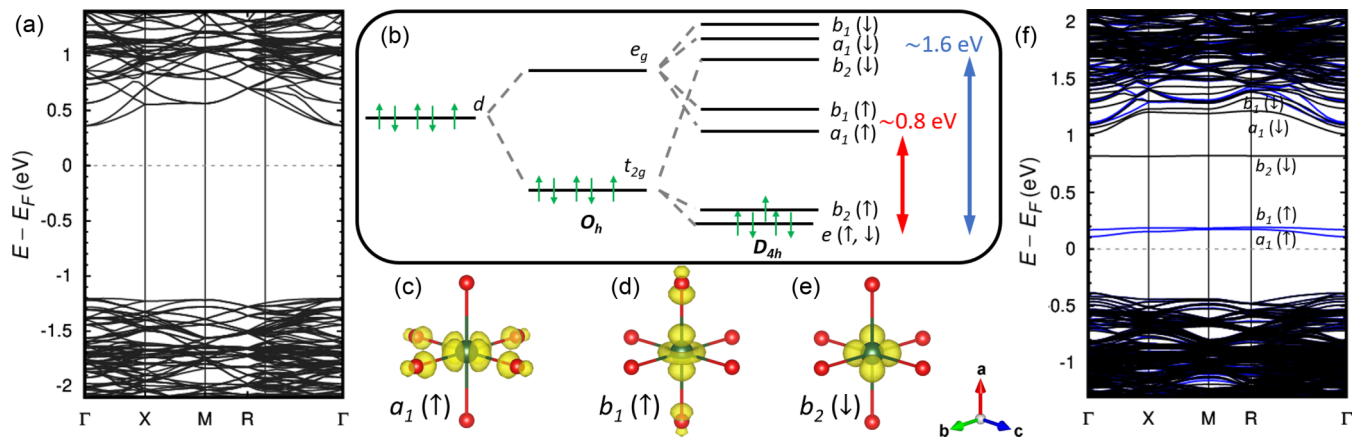


FIG. 4. (a) Pristine band structure of Co₃O₄ with a 224 atom supercell (primitive cell band structure shown in SM, Fig. S5). (b) Hole polarons create a low-spin (LS) d^5 configuration at Co(O) along with a Jahn-Teller (JT) distortion which results in a D_{4h} configuration and the creation of several midgap states. (c)–(e) Wave function isosurface plots (yellow cloud) of the three polaron induced states under hole formation of $a_1(\uparrow)(d_{x^2-y^2})$, $b_1(\uparrow)(d_{z^2})$, and $b_2(\downarrow)(d_{xy})$ character, respectively. Isosurface plots use a cutoff value of 10% the maximum. (f) Band structure of Co₃O₄ with a hole polaron which shows several induced gap states (blue = spin up; black = spin down).

We now turn to a more quantitative discussion of polaron effects on the electronic structure of Co₃O₄. In particular, we obtain a band gap of 1.6 eV and 1.7 eV with the current choice of U and α (respectively), which is in excellent agreement with the value of 1.5–1.7 eV reported in Refs. [42–48]. However, this is significantly larger than the result of 0.7–0.9 eV claimed by other experiments [49–52]. We note that exciton binding energies are usually less than 150 meV in many TMOs [23,74,75], and we show later that the calculated optical spectra, by including excitonic effects, cannot explain the low energy transition at 0.7–0.9 eV. Interestingly, as shown in Fig. 4(b), at the current level of theory, we find that the midgap states are located at 0.8 eV away from the valence band maximum and are associated with the hole polaron formation. This observation suggests that a scenario similar to the one observed for Fe₂O₃ may also occur in Co₃O₄, i.e., the true gap of Co₃O₄ is ~ 1.6 eV, and the midgap states are responsible for the transitions found at ~ 0.8 eV in the experimental optical absorption spectra [49–52]. In order to verify our hypothesis and to further elucidate the role of polaron formation, we calculated the optical absorption spectra of Co₃O₄ with and without a hole polaron, and we compared the results with available experimental data. Absorption spectrum with a hole polaron was computed with a 56-atom supercell [76], which better represents experimental hole concentrations of p -type Co₃O₄ [42,44] due to abundant cation vacancies [55,77].

Therefore, we computed the imaginary part of the dielectric function in the random phase approximation (RPA) with local field effects (as shown in Fig. 5) and solving the Bethe-Salpeter equation that includes excitonic effects (as shown in SM Figs. S8 and S9), as implemented in the YAMBO code [78], using the single particle eigenvalues and wave functions derived from DFT+ U . We note that this choice of starting point considers the balance between accuracy and computational cost, similar to the work in Ref. [79]. In addition, for a direct comparison with experimental measurements, we calculated the absorption coefficient from the

dielectric function [80]:

$$A(\omega) = \frac{\omega}{c} \frac{\epsilon_2(\omega)}{\sqrt{\epsilon_1(\omega) + \sqrt{\epsilon_1(\omega)^2 + \epsilon_2(\omega)^2}}}. \quad (1)$$

The calculated optical absorption spectra of Co₃O₄ are shown in Fig. 5, together with the experimental spectrum. We find that the introduction of hole polarons leads to the formation of several lower energy optical transition peaks

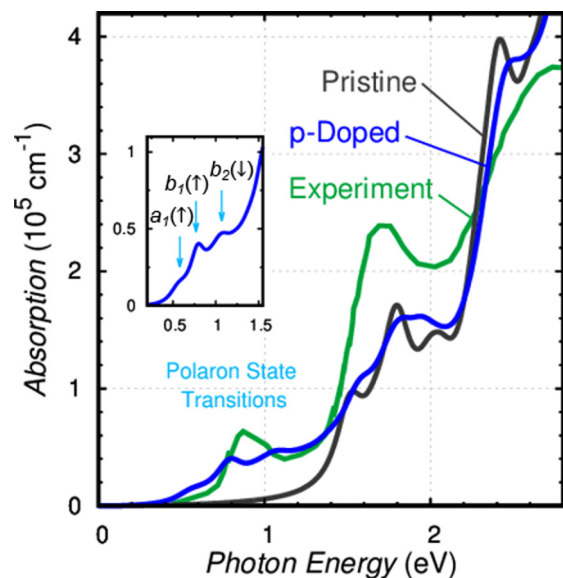


FIG. 5. Optical absorption of Co₃O₄ in the pristine system (black) and the p -doped system (blue). Notably, only p -type doping, i.e., the formation of holes, will cause midgap transitions below 1.6 eV, in agreement with experimental optical spectrum of Co₃O₄ shown in green [49]. The inset image displays the midgap transitions which are labeled according to the states formed from hole polaron formation as in Fig. 4. (Theoretical spectrum is an average of spectra with light polarized in the [100], [010], and [001] directions.)

between 0.6 and 1.2 eV in Co_3O_4 . More importantly, we find that, in sharp contrast to the result obtained for the pristine system, the spectrum computed for Co_3O_4 with a hole polaron is in very good agreement with experimental data, where three lower lying transitions were also found between 0.7 and 1.1 eV [42–44,49]. Our analysis indicates that these transitions can be associated with those occurring between the p - d hybridized dispersive valence states and the localized d states formed at the hole polaron site, for which the wave functions are illustrated in Figs. 4(c)–4(e). Collectively, these results clearly support the interpretation that the true optical gap of Co_3O_4 is ~ 1.6 eV and that the optical transitions observed at ~ 0.8 eV are due to hole polaron formation at Co(O) sites. We note that electron polarons do not lead to the formation of low lying transitions (see Fig. S6), indicative of the p -doped nature of the experimental system.

In order to rule out the possibility that the low energy transitions ~ 0.8 eV are caused by large excitonic effects [79,81–83], we also computed absorption spectra of pristine Co_3O_4 including excitonic effects by solving the Bethe-Salpeter equation, as shown in SM Figs. S7 and S8. More detailed discussions can be found in the SM. Overall, no extra peaks in the BSE spectra show up at the energy range below 1 eV for pristine Co_3O_4 (no hole polaron included), which confirms the excitonic effects do not explain the low energy transitions in the absence of SPs.

In addition, we note that we neglect electron-phonon coupling and thermal expansion effects on the band edge positions and absorption spectra at finite temperature, as discussed in Refs. [84,85]. In the presence of temperature effects, the absorption edge may be subject to a redshift and overall broadening of the spectra, which is the subject of our future studies. However, we expect that these effects will not lead to an additional peak that is well separated from the main absorption in a direct band-gap semiconductor like Co_3O_4 , and therefore our conclusion on the contribution of small polarons to the low energy optical transitions still holds.

Finally, we propose an experimentally viable method for distinguishing optical transitions involving localized polaron states from traditional band-band bulk state transitions. For Co_3O_4 , the JT distortion upon the introduction of the hole polaron extends the Co-O bonds along the C_4 axis, and this distortion may occur along any of the bond axis that aligns with the [100], [010], [001] directions of the cubic unit cell. Such a threefold degeneracy can be broken if uniaxial strain is applied to the system along one of the crystal lattice directions, which in turn may affect the optical absorption spectrum. In this regard, monitoring the change in the optical spectrum of Co_3O_4 in the presence of a uniaxial strain could potentially provide signatures of hole polarons associated with a specific JT distortion.

For demonstration, we considered a 1% tensile strain applied along the [100] direction. We find that the threefold degeneracy in the polaron states is broken upon the introduction of the strain; in particular, polaron formation with the JT elongation along the [100] direction is lowered in the energy by 5 meV compared to those associated with the [010] or [001] directions. Here, to investigate the collective and individual effects of these polarons on the absorption spectrum, we computed a thermally averaged ensemble spectrum

by using a Boltzmann probability distribution of the optical absorption obtained for each case:

$$P_i = \frac{e^{E_i/kT}}{\sum_i e^{E_i/kT}}, \quad A(\omega) = \sum_i P_i A_i(\omega), \quad (2)$$

where E_i and A_i are the energy and absorption spectrum of the system containing a polaron in the state i (i denotes different JT elongation directions), respectively.

The calculated optical absorption spectrum presented in Fig. 6 clearly shows a redshift in the first peak that is associated with polarons. In particular, we find that at lower temperatures where kT is on the order of 5 meV or less, the resulting optical spectra follow that of the lowest energy polaron associated with JT elongation along the [100] direction. At higher temperatures, the clear redshift remains, although a high temperature of 300 K is sufficient to quench the 5 meV energy difference between polaron states. In contrast to the transition associated with hole polarons, we find that bulk band-band transitions at higher energy (above 1.5 eV) remain mostly unchanged upon uniaxial strain (see Fig. S9). Accordingly, this allows one to clearly distinguish the local polaron state involved in optical transitions, whose JT distortion renders them quite sensitive to strain, from that of the band-band bulk state transitions which are insensitive to strain.

To summarize, we present a detailed investigation of the electronic structure and polaronic induced optical transitions in Co_3O_4 based on first-principles calculations. We resolved several contradicting findings in the literature related to the character of the charge carrier and band gap of the material. In particular, we show that the optical gap of pristine Co_3O_4 is 1.6 eV, whereas the lower lying transition around ~ 0.8 eV is associated with the hole polaron, which was misinterpreted as the band edge of the material. We also demonstrated the

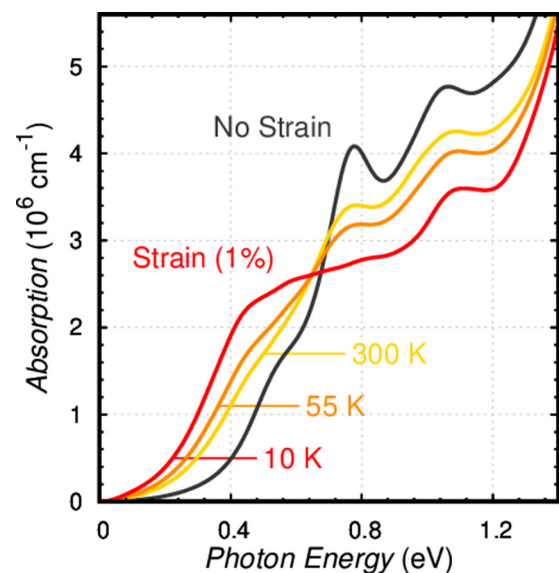


FIG. 6. Optical absorption of p -doped Co_3O_4 under 1% uniaxial tensile strain along the [100] direction. Temperature dependence determines the probability for which direction the Jahn-Teller elongation will occur (as the degeneracy is removed under strain) and results in a redshift of optical peaks related to the hole polaron.

important effects of uniaxial strain on the optical spectra of Co_3O_4 , which in turn can be used to reveal the localized character of polaron-induced electronic states.

Our study also suggests a strategy for establishing a potential first-principles approach that can simultaneously achieve an accurate description of polaron states, electronic band structure, and optical properties in polaronic magnetic oxides. Specifically, the generalized Koopmans' condition can be utilized to derive the fraction of exact exchange from first principles, which in turn can be used in hybrid functionals for investigating the electronic structure of the oxide. These hybrid functionals can also be used for benchmarking DFT- U calculations, which offer a much lower computational cost, or to provide inputs for higher level electronic structure methods, such as many-body perturbation theory within the GW approximation.

This work was performed under the auspices of the US Department of Energy by Lawrence Livermore National

Laboratory under Contract No. DEAC5207NA27344. T.J.S., T.A.P., and T.O. are supported by the US Department of Energy, Office of Energy Efficiency and Renewable Energy, Fuel Cell Technologies Office. Y.P. is supported by the National Science Foundation under Grants No. DMR-1760260 and No. CHE-1904547. This research used computational support from the LLNL Grand Challenge Program, the Center for Functional Nanomaterials, which is a US DOE Office of Science Facility, and the Scientific Data and Computing center, a component of the Computational Science Initiative, at Brookhaven National Laboratory under Contract No. DE-SC0012704, the National Energy Research Scientific Computing Center (NERSC), a US Department of Energy Office of Science User Facility operated under Contract No. DE-AC02-05CH11231, and the Extreme Science and Engineering Discovery Environment (XSEDE), which is supported by National Science Foundation Grant No. ACI-1548562 [86]. We acknowledge fruitful discussion with Lin-Wang Wang and Di-Jia Liu.

-
- [1] M. Reticioli, U. Diebold, G. Kresse, and C. Franchini, *Handbook of Materials Modeling: Applications: Current and Emerging Materials* (Springer International Publishing, Cham, 2019), pp. 1–39.
- [2] K. Sivula, F. Le Formal, and M. Grätzel, *ChemSusChem* **4**, 432 (2011).
- [3] Y. Ling, G. Wang, D. A. Wheeler, J. Z. Zhang, and Y. Li, *Nano Lett.* **11**, 2119 (2011).
- [4] T. J. Smart and Y. Ping, *J. Phys.: Condens. Matter* **29**, 394006 (2017).
- [5] M. Gong, W. Zhou, M.-C. Tsai, J. Zhou, M. Guan, M.-C. Lin, B. Zhang, Y. Hu, D.-Y. Wang, J. Yang *et al.*, *Nat. Commun.* **5**, 4695 (2014).
- [6] C. Hu, K. Chu, Y. Zhao, and W. Y. Teoh, *ACS Appl. Mater. Interfaces* **6**, 18558 (2014).
- [7] Z. Wang, H. Liu, R. Ge, X. Ren, J. Ren, D. Yang, L. Zhang, and X. Sun, *ACS Catal.* **8**, 2236 (2018).
- [8] A. Aijaz, J. Masa, C. Rösler, W. Xia, P. Weide, A. J. Botz, R. A. Fischer, W. Schuhmann, and M. Muhler, *Angew. Chem., Int. Ed. Engl.* **55**, 4087 (2016).
- [9] K. Jin, A. Chu, J. Park, D. Jeong, S. E. Jerng, U. Sim, H.-Y. Jeong, C. W. Lee, Y.-S. Park, K. D. Yang *et al.*, *Sci. Rep.* **5**, 10279 (2015).
- [10] F. Wu and Y. Ping, *J. Mater. Chem. A* **6**, 20025 (2018).
- [11] W. Zhang, F. Wu, J. Li, D. Yan, J. Tao, Y. Ping, and M. Liu, *ACS Energy Lett.* **3**, 2232 (2018).
- [12] H. Seo, Y. Ping, and G. Galli, *Chem. Mater.* **30**, 7793 (2018).
- [13] T. W. Kim, Y. Ping, G. A. Galli, and K.-S. Choi, *Nat. Commun.* **6**, 8769 (2015).
- [14] A. C. Cardiel, K. J. McDonald, and K.-S. Choi, *Langmuir* **33**, 9262 (2017).
- [15] T. J. Smart, A. C. Cardiel, F. Wu, K.-S. Choi, and Y. Ping, *npj Comput. Mater.* **4**, 61 (2018).
- [16] D. K. Lee, D. Lee, M. A. Lumley, and K.-S. Choi, *Chem. Soc. Rev.* **48**, 2126 (2019).
- [17] Y. Tachibana, L. Vayssieres, and J. R. Durrant, *Nat. Photon.* **6**, 511 (2012).
- [18] I. Roger, M. A. Shipman, and M. D. Symes, *Nat. Rev. Chem.* **1**, 0003 (2017).
- [19] Y. Yan, B. Y. Xia, B. Zhao, and X. Wang, *J. Mater. Chem. A* **4**, 17587 (2016).
- [20] P. Liao and E. A. Carter, *Chem. Soc. Rev.* **42**, 2401 (2013).
- [21] N. Mott, *J. Non-Cryst. Solids* **1**, 1 (1968).
- [22] M. Gerosa, F. Gygi, M. Govoni, and G. Galli, *Nat. Mater.* **17**, 1122 (2018).
- [23] Y. Ping, D. Rocca, and G. Galli, *Phys. Rev. B* **87**, 165203 (2013).
- [24] B. Yan, D. Wan, X. Chi, C. Li, M. R. Motapothula, S. Hooda, P. Yang, Z. Huang, S. Zeng, A. G. Ramesh *et al.*, *ACS Appl. Mater. Interfaces* **10**, 38201 (2018).
- [25] S. Moser, L. Moeschini, J. Jaćimović, O. S. Barišić, H. Berger, A. Magrez, Y. J. Chang, K. S. Kim, A. Bostwick, E. Rotenberg *et al.*, *Phys. Rev. Lett.* **110**, 196403 (2013).
- [26] W. Kang and M. S. Hybertsen, *Phys. Rev. B* **82**, 085203 (2010).
- [27] C. Verdi, F. Caruso, and F. Giustino, *Nat. Commun.* **8**, 15769 (2017).
- [28] Z. Wang, S. McKeown Walker, A. Tamai, Y. Wang, Z. Ristic, F. Y. Bruno, A. de la Torre, S. Riccò, N. C. Plumb, M. Shi *et al.*, *Nat. Mater.* **15**, 835 (2016).
- [29] L. M. Carneiro, S. K. Cushing, C. Liu, Y. Su, P. Yang, A. P. Alivisatos, and S. R. Leone, *Nat. Mater.* **16**, 819 (2017).
- [30] S. Biswas, J. Husek, S. Londo, and L. R. Baker, *J. Phys. Chem. Lett.* **9**, 5047 (2018).
- [31] C. Lohaus, A. Klein, and W. Jaegermann, *Nat. Commun.* **9**, 4309 (2018).
- [32] M. N. Huda, A. Walsh, Y. Yan, S.-H. Wei, and M. M. Al-Jassim, *J. Appl. Phys.* **107**, 123712 (2010).
- [33] O. Neufeld and M. C. Toroker, *J. Phys. Chem. C* **119**, 5836 (2015).
- [34] A. Sanson, A. Zaltron, N. Argiolas, C. Sada, M. Bazzan, W. G. Schmidt, and S. Sanna, *Phys. Rev. B* **91**, 094109 (2015).
- [35] N. Yatom, O. Neufeld, and M. Caspary Toroker, *J. Phys. Chem. C* **119**, 24789 (2015).

- [36] Z.-S. Wu, W. Ren, L. Wen, L. Gao, J. Zhao, Z. Chen, G. Zhou, F. Li, and H.-M. Cheng, *ACS Nano* **4**, 3187 (2010).
- [37] W.-Y. Li, L.-N. Xu, and J. Chen, *Adv. Funct. Mater.* **15**, 851 (2005).
- [38] T. Y. Ma, S. Dai, M. Jaroniec, and S. Z. Qiao, *J. Am. Chem. Soc.* **136**, 13925 (2014).
- [39] M. Hamdani, R. N. Singh, and P. Chartier, *Int. J. Electrochem. Sci.* **5**, 556 (2010).
- [40] S. K. Meher and G. R. Rao, *J. Phys. Chem. C* **115**, 15646 (2011).
- [41] X.-h. Xia, J.-p. Tu, Y.-j. Mai, X.-l. Wang, C.-d. Gu, and X.-b. Zhao, *J. Mater. Chem.* **21**, 9319 (2011).
- [42] C. Lohaus, J. Morasch, J. Brötz, A. Klein, and W. Jaegermann, *J. Phys. D: Appl. Phys.* **49**, 155306 (2016).
- [43] C.-M. Jiang, L. R. Baker, J. M. Lucas, J. Vura-Weis, A. P. Alivisatos, and S. R. Leone, *J. Phys. Chem. C* **118**, 22774 (2014).
- [44] M. M. Waegle, H. Q. Doan, and T. Cuk, *J. Phys. Chem. C* **118**, 3426 (2014).
- [45] V. Shinde, S. Mahadik, T. Gujar, and C. Lokhande, *Appl. Surf. Sci.* **252**, 7487 (2006).
- [46] I. Belova, Y. E. Roginskaya, R. Shifrina, S. Gagarin, Y. V. Plekhanov, and Y. N. Venevtsev, *Solid State Commun.* **47**, 577 (1983).
- [47] A. Lima, *J. Phys. Chem. Solids* **75**, 148 (2014).
- [48] C.-S. Cheng, M. Serizawa, H. Sakata, and T. Hirayama, *Mater. Chem. Phys.* **53**, 225 (1998).
- [49] L. Qiao, H. Y. Xiao, H. Meyer, J. Sun, C. M. Rouleau, A. A. Puretzy, D. B. Geohegan, I. N. Ivanov, M. Yoon, W. J. Weber *et al.*, *J. Mater. Chem. C* **1**, 4628 (2013).
- [50] V. Singh, M. Kosa, K. Majhi, and D. T. Major, *J. Chem. Theory Comput.* **11**, 64 (2014).
- [51] O. Sousa, J. Lima, A. Lima, and M. Lalic, *J. Magn. Magn. Mater.* **484**, 21 (2019).
- [52] J. Martens, W. Peeters, H. Van Noort, and M. Erman, *J. Phys. Chem. Solids* **46**, 411 (1985).
- [53] D. A. Wheeler, G. Wang, Y. Ling, Y. Li, and J. Z. Zhang, *Energy Environ. Sci.* **5**, 6682 (2012).
- [54] P. H. T. Ngamou and N. Bahlawane, *Chem. Mater.* **22**, 4158 (2010).
- [55] F. Tronel, L. Guerlou-Demourgues, M. Ménétrier, L. Croguennec, L. Goubault, P. Bernard, and C. Delmas, *Chem. Mater.* **18**, 5840 (2006).
- [56] P. Sahoo, H. Djieutedjeu, and P. F. Poudeu, *J. Mater. Chem. A* **1**, 15022 (2013).
- [57] T. D. Sparks, A. Gurlo, M. W. Gaultois, and D. R. Clarke, *Phys. Rev. B* **98**, 024108 (2018).
- [58] K. Koumoto and H. Yanagida, *J. Am. Ceram. Soc.* **64**, C156 (1981).
- [59] S. L. Dudarev, G. A. Botton, S. Y. Savrasov, C. J. Humphreys, and A. P. Sutton, *Phys. Rev. B* **57**, 1505 (1998).
- [60] P. R. Kent and G. Kotliar, *Science* **361**, 348 (2018).
- [61] G. Miceli, W. Chen, I. Reshetnyak, and A. Pasquarello, *Phys. Rev. B* **97**, 121112(R) (2018).
- [62] T. J. Smart, F. Wu, M. Govoni, and Y. Ping, *Phys. Rev. Materials* **2**, 124002 (2018).
- [63] Q. Liu, Q. Yao, Z. A. Kelly, C. M. Pasco, T. M. McQueen, S. Lany, and A. Zunger, *Phys. Rev. Lett.* **121**, 186402 (2018).
- [64] S. Lany, *Phys. Status Solidi B* **248**, 1052 (2011).
- [65] See Supplemental Material at <http://link.aps.org/supplemental/10.1103/PhysRevMaterials.3.102401> for details of electron polaron formation, the choice of DFT+*U* values, supercell comparison, electronic structure of pristine Co₃O₄, other origins of midgap transitions, absorption spectra computed by BSE and RPA approximations, and further effect of strain on optical spectra.
- [66] T. Bischoff, I. Reshetnyak, and A. Pasquarello, *Phys. Rev. B* **99**, 201114(R) (2019).
- [67] P. Giannozzi, S. Baroni, N. Bonini, M. Calandra, R. Car, C. Cavazzoni, D. Ceresoli, G. L. Chiarotti, M. Cococcioni, I. Dabo *et al.*, *J. Phys.: Condens. Matter* **21**, 395502 (2009).
- [68] D. R. Hamann, *Phys. Rev. B* **88**, 085117 (2013).
- [69] R. Sundararaman and Y. Ping, *J. Chem. Phys.* **146**, 104109 (2017).
- [70] S. Kokott, S. V. Levchenko, P. Rinke, and M. Scheffler, *New J. Phys.* **20**, 033023 (2018).
- [71] W. Roth, *J. Phys. Chem. Solids* **25**, 1 (1964).
- [72] J. Chen, X. Wu, and A. Selloni, *Phys. Rev. B* **83**, 245204 (2011).
- [73] M.-S. Wu, B. Xu, and C.-Y. Ouyang, *J. Mater. Sci.* **51**, 4691 (2016).
- [74] Y. Ping, D. Rocca, and G. Galli, *Chem. Soc. Rev.* **42**, 2437 (2013).
- [75] T. Le Bahers, M. Rérat, and P. Sautet, *J. Phys. Chem. C* **118**, 5997 (2014).
- [76] The typical concentration of cobalt vacancies is 5% [55,77], which corresponds to a hole concentration of 10% and 15% for Co(T) and Co(O) vacancies, respectively. In this regard, it is reasonable to simulate hole polarons in Co₃O₄ using a 56-atom supercell that yields a hole concentration of 12.5% for a proper representation of the experimental systems.
- [77] G. Godillot, L. Guerlou-Demourgues, L. Croguennec, K. Shaju, and C. Delmas, *J. Phys. Chem. C* **117**, 9065 (2013).
- [78] A. Marini, C. Hogan, M. Grüning, and D. Varsano, *Comput. Phys. Commun.* **180**, 1392 (2009).
- [79] C. Rödl and F. Bechstedt, *Phys. Rev. B* **86**, 235122 (2012).
- [80] J. D. Jackson, *Classical Electrodynamics* (Wiley, New York, 1999).
- [81] R. Laskowski, N. E. Christensen, P. Blaha, and B. Palanivel, *Phys. Rev. B* **79**, 165209 (2009).
- [82] F. Bruneval, N. Vast, L. Reining, M. Izquierdo, F. Sirotti, and N. Barrett, *Phys. Rev. Lett.* **97**, 267601 (2006).
- [83] J. Wiktor, I. Reshetnyak, M. Strach, M. Scarongella, R. Buonsanti, and A. Pasquarello, *J. Phys. Chem. Lett.* **9**, 5698 (2018).
- [84] B. Monserrat, C. E. Dreyer, and K. M. Rabe, *Phys. Rev. B* **97**, 104310 (2018).
- [85] I. Bravić and B. Monserrat, *Phys. Rev. Materials* **3**, 065402 (2019).
- [86] J. Towns, T. Cockerill, M. Dahan, I. Foster, K. Gaiher, A. Grimshaw, V. Hazlewood, S. Lathrop, D. Lifka, G. D. Peterson *et al.*, *Comput. Sci. Eng.* **16**, 62 (2014).